Tuning interfacial energy barriers in heterojunctions for anti-interference sensing

Minggang Zhao[a], Jiatuo Yu[a], Xiaomin Zhang[a], Zhengming Li[a], Yu Ding[a], Ye Ma[a]* and Hui Li[b]*

[a]Department of Materials Science and Engineering, Ocean University of China, Qingdao, 266100, People's Republic of China

[b]Optoelectronic Materials and Technologies Engineering Laboratory of Shandong, Physics Department, Qingdao University of Science and Technology, Qingdao, 266100, People's Republic of China

*E-mail: zhaomg@ouc.edu.cn

ABSTRACT:

Analytes with similar redox properties are normally difficult to distinguish through classic electrochemical methods. This becomes especially true for the on-site detection in seawater where the high salinity and complex chemical components can impose severe interference. Hereby introducing numerous nanoscale heterojunctions in the Cu/CuO/reduced graphene oxide (rGO)/polypyrrole and Cu/CuO/rGO/chitosan electrochemical sensors, we can construct tunable interfacial energy barriers to exponentially regulate the electrochemical signal. Importantly, these energy barriers are independent to redox but closely related to the electrostatic induction oriented from specifically absorbed charged analytes such as Hg^{2+} and Cu^{2+}. Moreover, the similar sensing principle is also valid for the energy barriers in p-n junctions as demonstrated in the Ni/NiO/ZnO/ Polypyrrole sensor. The good anti-interference properties and

ultrahigh sensitivity of the new sensing mode offer new opportunities in trace analyte detection in harsh environments such as seawater.

KEYWORDS: *Semiconductor, Heterojunction, Nano-interfaces, Energy barrier, Sensor*

Oceans are a great treasure trove of resources and the birthplace of life on earth. However, the coastal seawater pollution is becoming increasingly serious with the development of the economy. Therefore, real-time field monitoring is required now for more effective control of pollution. However, due to the high salinity and the complex components of seawater, strong interference has plagued the in-field seawater sensors.[1] Some sophisticated pretreatments of the samples, such as digestion, separation and purification, are thus needed to minimize these matrix effects, which makes detection complicated and time consuming.[2,3] Therefore, it is urgent and challenging to achieve a good property of anti-interference.

Heavy metals in seawater can cause huge threats to human health, marine organisms and ecosystem even at low concentrations.[4] Among methods of heavy metal detection, electrochemistry is a facile method with high sensitivity, low cost, fast response and simplicity, which is widely used in the determination of heavy metals.[5-8] However, as mentioned above, the presence of different kinds of interfering species in seawater renders the direct electrochemical detection of heavy metals extremely hard. Specifically, the traditional sensors based on electrochemical redox can be easily interfered by the electrochemical active substances with similar redox properties.[9] Though introducing specially designed ligands that have high affinity to the analytes

can boost the target signal, the interfering redox signals persist in the electrochemical background. New methods of anti-interference in electrochemical sensing are still needed.

Recently, the rational design of heterojunction interfaces has achieved excellent performance in various research fields, such as sensors, catalysis, solar energy, etc.[10-12] Especially, the interfacial electronic effects of a semiconductor can afford more handles for tuning electron transport.[13-15] For example, through obstructing the pathway of electrons, the interfacial energy barriers can give rise to the nonlinear impedance characteristics of heterojunctions,[16-19] which can produce corresponding electrochemical current responses. In addition, these energy barriers are usually regulated by physical factors such as stress, light and especially electrostatic induction, which are independent to electrochemical redox and hard to be disturbed by those interfering species. Therefore, different analytes could generate similar electrochemical redox signals, the physical electrostatic interactions between the analytes and the heterojunction interfaces could be different. These electrostatic interactions independent to redox can have a major impact on the interfacial energy barriers which regulate the electrochemical signals and at last differentiate the targets from interfering species.

By utilizing the different advanced sensing materials such as reduced graphene oxide (rGO), p-type CuO, p-type NiO and n-type ZnO, we constructed different hierarchical structures such as Cu/CuO/rGO and Ni/NiO/ZnO, and successfully introduced different interfacial energy barriers of Schottky or p-n junctions into the

electrochemical sensors. Through the electrostatic interactions between the charged analytes and the interfacial junctions, the height of the energy barriers can be modified corresponding to the different charged analytes, which at last can be exponentially reflected in the electrochemical responses of the sensors. The specifically designed absorbing layer such as polypyrrole (PPy) for Hg^{2+} and chitosan (CS) for Cu^{2+} can accumulate analytes and their charges whose electrostatic induction can influence the interfacial energy barrier even without involving redox. The good anti-interference properties and ultrahigh sensitivity of the new sensing mode offer new opportunities in trace analyte detection in harsh environments such as seawater.

RESULTS AND DISCUSSION

It is known that the work function of rGO is lower than that of p-type CuO semiconductor (Figure 1a), therfore at an equilibrium state, the energy bands of CuO will bend downward forming a Schottky junction[20] (Figure 1b). According to the interfacial theory of semiconductor, the interfacial energy barrier (Φ_B) obstructs the transport of electrons from rGO to CuO. The obstruction effect on electrons transport is directly reflected on the corresponding current through the Schottky junction, which is described as $J = AT^2\exp(-q\Phi_B/kT)[\exp(qV/kT)-1]$, where A is effective Richardson constant, T is the absolute temperature, V is the bias applied voltage, q is charge and k is Boltzmann constant.[21-24] From the equation, it is found that the change of the height of the energy barrier, $\Delta\Phi_B$, can exponentially magnify the current responses, which lays the foundation of the new sensing mode. In an electrochemical process, the obstruction effect and $\Delta\Phi_B$ can be also reflected in the electrochemical impedance. More

importantly, $\Delta\Phi_B$ can be influenced by various physical triggers such as stress, light and electrostatic induction that are independent to electrochemical redox. Therefore, through physically tuning the interfacial energy barriers Φ_B, it is promising to build a high-performance sensor with good specificity.

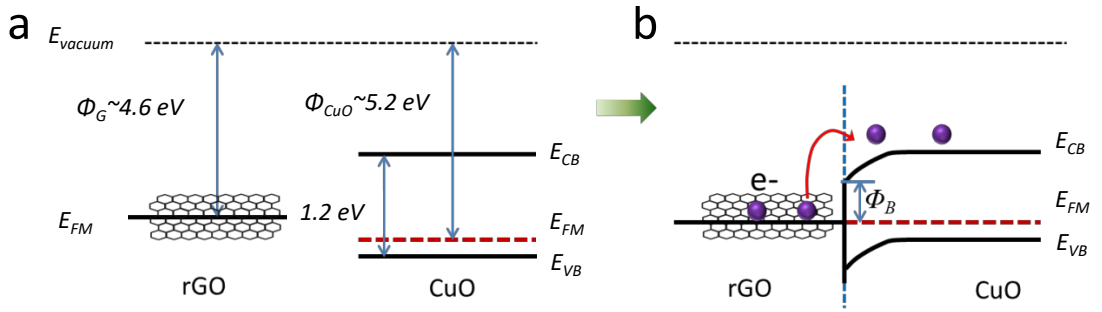

Figure 1. a) The energy band structures of rGO and p-CuO semiconductor. The work function of rGO (Φ_G) is about 4.6 eV, while the work function of CuO (Φ_b) is about 5.2 eV. E_{FM} stands for Fermi energy, E_{CB} for energy of conducting band, E_{VB} for valence band. b) When the two materials contact with each other, at an equilibrium state, the energy bands of CuO will bend downward forming a Schottky junction with an energy barrier Φ_B for the electrons.

Cu/CuO/rGO wires were fabricated as a prototype demonstrating this novel sensing mode. Commercial Cu wires were surface-oxidized to form the Cu/CuO wires (diameter~300 μm) (Figure 2a) with a uniform surface covered by the cross-connected CuO nanowires (Figure 2b). A large number of Schottky interfaces (rGO/CuO) form after further the electro-deposition of the scattered rGO sheets (Figure 2c-e), introducing the energy barriers Φ_B. A rectification characteristic of the Cu/CuO/rGO wire was found in the I-V test by a sourcemeter in air (Figure 2f), indicating the energy barrier was successfully built. XRD patterns (Figure S1) of the Cu/CuO/rGO wire reveal the characteristic peaks of Cu and CuO. The weak intensity of CuO peaks is because the formed CuO layer is much thinner than the macroscale Cu wire.

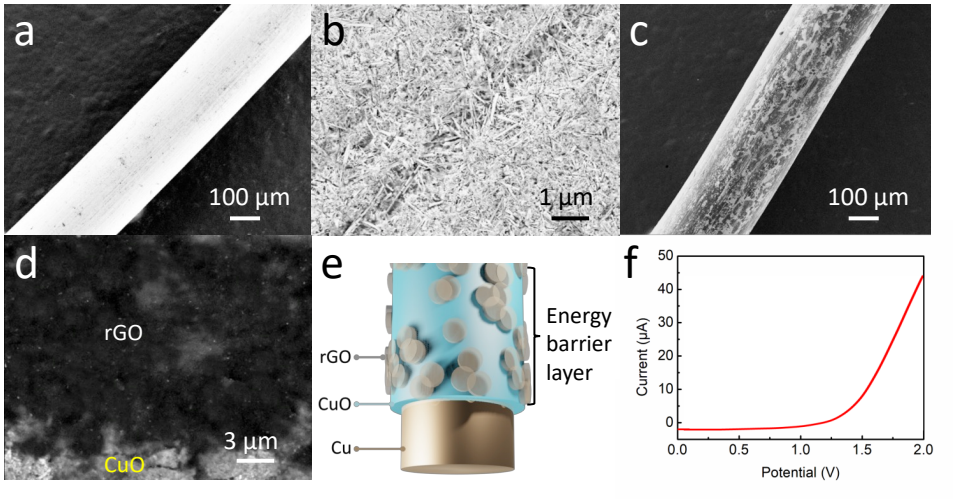

Figure 2. a) The low magnification SEM image of the Cu/CuO wire. b) The locally magnified SEM image of the Cu/CuO wire. c) The low magnification SEM image of the Cu/CuO/rGO wire. d) The locally magnified SEM image of the Cu/CuO/rGO wire. e) The schematic diagram of the Cu/CuO/rGO wire. f) The typical I–V curve of the Cu/CuO/rGO wire in air confirming the existence of the Schottky junction.

It is known that electrostatic induction is a physical phenomenon that can change the charge distribution and the energy band structure of semiconductors. For example, the electrostatic induced charge can change the band position of the exposed CuO in the Cu/CuO/rGO wire. Therefore, electrostatic induction is chosen as the physical trigger for producing $\Delta\Phi_B$. Hemoglobin (Hb) with an isoelectric point (pI) of 7.4 [25] is employed as the charged object for producing electrostatic induction, as it is positively charged when pI > pH, negatively charged when pI < pH and electrically neutral when pI = pH.[26] To demonstrate that the electrochemical sensing can be coupled with physical electrostatic induction through tuning the interfacial energy barrier Φ_B, Cu/CuO/rGO wire is constructed as a prototype sensor for dopamine (DA). It is found that the electrochemical oxidation peak current of DA increases remarkably with the addition of positively charged Hb (Figure 3a) but decreases significantly with the addition of negatively charged Hb (Figure 3c). No noticeable current change can be found with the

addition of electrically neutral Hb (Figure 3b). The above results demonstrate electrochemical responses can be adjusted by the physical electrostatic induction produced by the charged Hb.

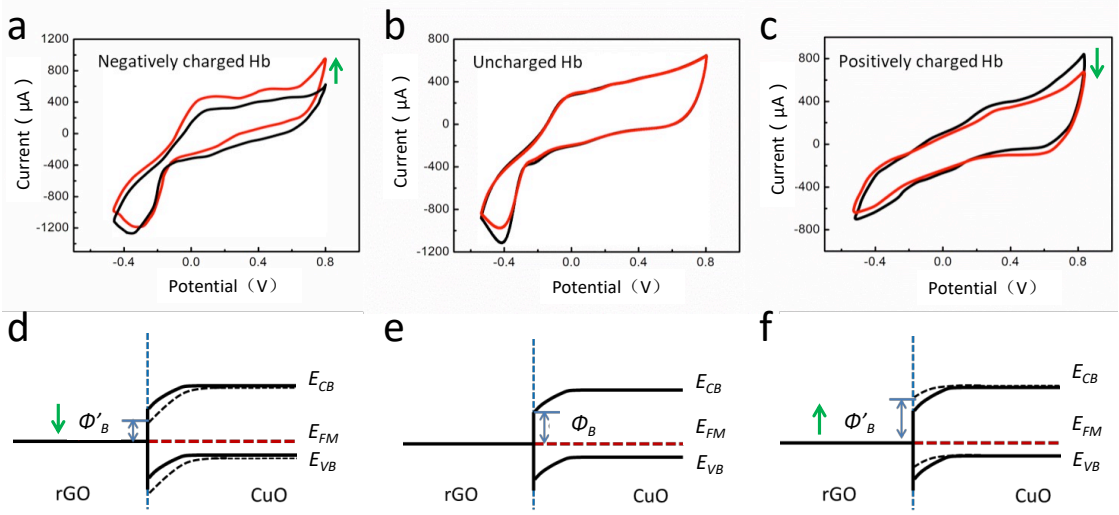

Figure 3. a-c) The change of oxidation peak current with the addition of different charged Hb, black curve: before adding Hb, red curve: after adding. a) adding positively charged Hb, b) adding uncharged Hb, c) adding negatively charge Hb. d-f) The corresponding change of Φ_B.

This phenomenon can be explained by the energy band diagrams (Figure 3d-f). The original Φ_B is determined by the difference of the work functions between rGO and CuO (Figure 3e). Positively charged Hb can induce negative charges in the exposed CuO due to electrostatic induction, which lowers the conduction band of CuO and decreases Φ_B (Figure 3d). As a result, the electrochemical impedance decreases and the electrochemical current increases. Correspondingly, negatively charged Hb can induce positive charges, which increases Φ_B (Figure 3f) and decreases the electrochemical current. Uncharged Hb cannot induce $\Delta\Phi_B$, so neglectable current response is observed (Figure 3e). The results are supported by the electrochemical impedance test (Figure S2). The above discussions demonstrate Φ_B can be used as an effective tuning factor to couple the electrochemical response and the electrostatic induction together.

Control experiments based on the above tests were further performed. For the Cu/rGO wire, the Cu/CuO wire without rGO and the Cu/CuO wire with fully covered rGO, no significant electrochemical response is observed at various pH values (Table S1), excluding the effects of pH and Hb itself. As for the Cu/CuO wire fully covered by rGO, since the rGO film prevents Hb being absorbed on the CuO surface, the electrostatic induction from Hb cannot influence the energy barrier on the CuO side. Namely, Φ_B exists but $\Delta\Phi_B \equiv 0$. The results demonstrate the electrochemical response is initiated by the physical electrostatic induction on the CuO surface from Hb. As for the Cu/CuO wire and the Cu/rGO wire, the lack of Schottky junctions precludes the possibility of tuning the interfacial energy barrier. Therefor these two control groups exhibit no response to Hb.

As an example, the direct electrochemical detection of heavy metals is proposed to demonstrate the potential application of the physical-electrochemical sensing mode. The above fabricated Cu/CuO/rGO wire is further coated by a layer of polypyrrole (PPy) for detection of Hg^{2+}, as its -NH- functional group has a selective binding affinity to Hg^{2+}.[27-28] The overall composite metal wire has strong mechanical stability and flexibility, which can be conveniently bent with various shapes (Figure 4a, Figure S3). The surface of the Cu/CuO/rGO wire became much rougher after being modified by PPy (Figure 4b). C element appears after the deposition of rGO and N element appears after deposition of PPy (Figure S4), indicating the successful fabrication of the hierarchical structure. From the peeled surface of the Cu/CuO/rGO/PPy wire (Figure 4c, Figure S5), we can see a sandwich structure where the CuO nanowires porous layer

(about 5 μm thick) is interlinked with Cu and rGO/PPy layer. This hierarchical structure can be divided into 3 functional layers (Figure 4d): the inner Cu core as a high-speed electronic channel; the outermost PPy layer for the selective adsorption of Hg^{2+}; and the middle layer (CuO/rGO) as the heterojunction for constructing the energy barriers.

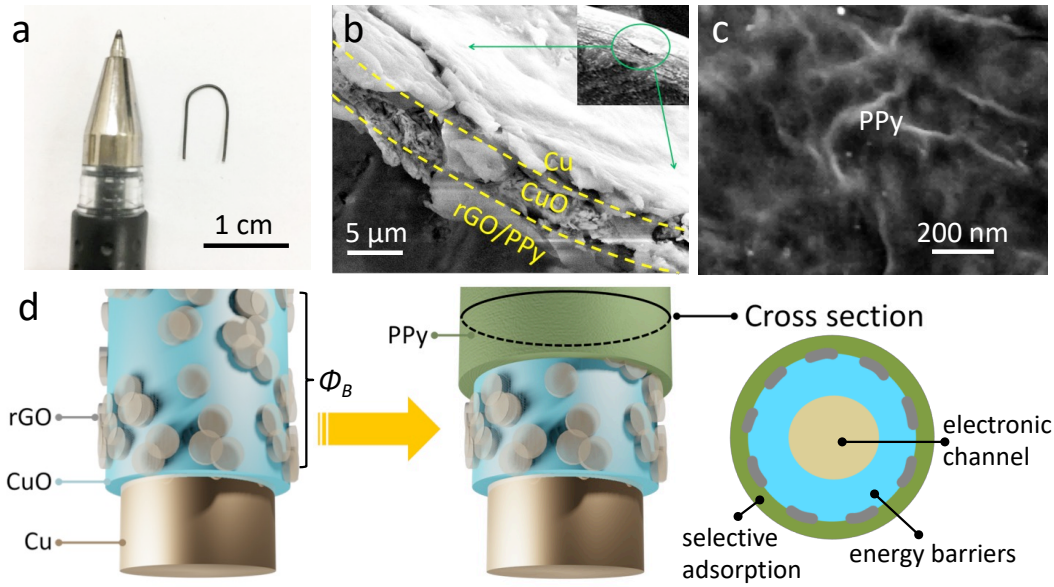

Figure 4. a) The macroscale photo of the Cu/CuO/rGO/PPy wire. b) The locally magnified SEM image of the peeled surface of the Cu/CuO/rGO wire. c) The macroscopic image of the prepared Cu/CuO/rGO/PPy wire with U shape. d) The schematic diagram of the Cu/CuO/rGO/PPy wire. The Cu wire (brown cylinder) in the core acts as the electron transport channel; the CuO (blue shell) and the rGO (semitransparent grey tablets) act as the heterojunction; the PPy (the outmost green shell) as the selective adsorption layer.

The Φ_B based physical-electrochemical sensing mode for detection of Hg^{2+} is shown in the schematic diagram (Figure 5). The specific adsorption of Hg^{2+} on PPy forms a positively charged layer due to charge conservation. As the formed positively charged layer is connected to the surface of the composite metal wire, it is prone to trap electrons from the exposed CuO by electrostatic interaction. As a result, the conduction band of CuO lifts and Φ_B increases, which increases the electrochemical impedance and decreases the electrochemical current. The more Hg^{2+} is adsorbed, the more the electrochemical current decreases, so the direct electrochemical detection of Hg^{2+} can

be achieved.

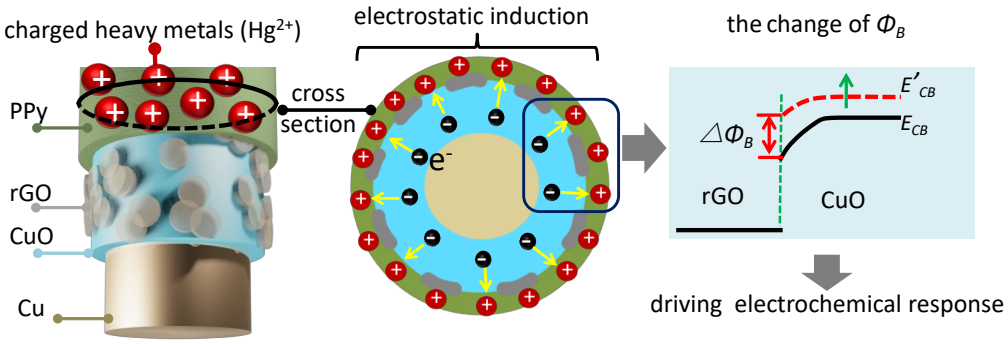

Figure 5. The schematic diagram of the physical-electrochemical sensing mode for detection of heavy metals (Hg^{2+}). After the specific adsorption of Hg^{2+} on the PPy layer, the formed positively charged layer traps electrons from the exposed CuO by electrostatic interaction, which raises the conducting band of CuO, increases the Φ_B.

Control experiments were carried out to verify the above sensing mode for detecting Hg^{2+}. The fabricated Cu/CuO/rGO/PPy wires with different amount of rGO (sample 1: slightly coated with rGO after 30 s electrodeposition; sample 2: partially coated with rGO after 60 s electrodeposition, as discussed in the above model; sample 3: fully coated with rGO after 100 s electrodeposition) exhibit different performance in Hg^{2+} detection. As shown in Figure 6, for sample 1, since the coverage of the CuO/rGO Schottky junctions is much less than that of the bare CuO, the electrochemical current passing through the bare CuO dominates. For sample 3, Hg^{2+} can hardly trap electrons from CuO to produce $\Delta\Phi_B$ due to the shielding of the fully covered rGO layer. Only in sample 2, a significant electrochemical response can be witnessed, because the coverage of rGO is high enough to form the Schottky junctions that regulate electrochemical currents, but not too high to shield the electrostatic interactions between the PPy/Hg^{2+} and the CuO. Therefore, to obtain optimum sensitivity, the coverage of the rGO, namely the Schottky junctions plays a critical role.

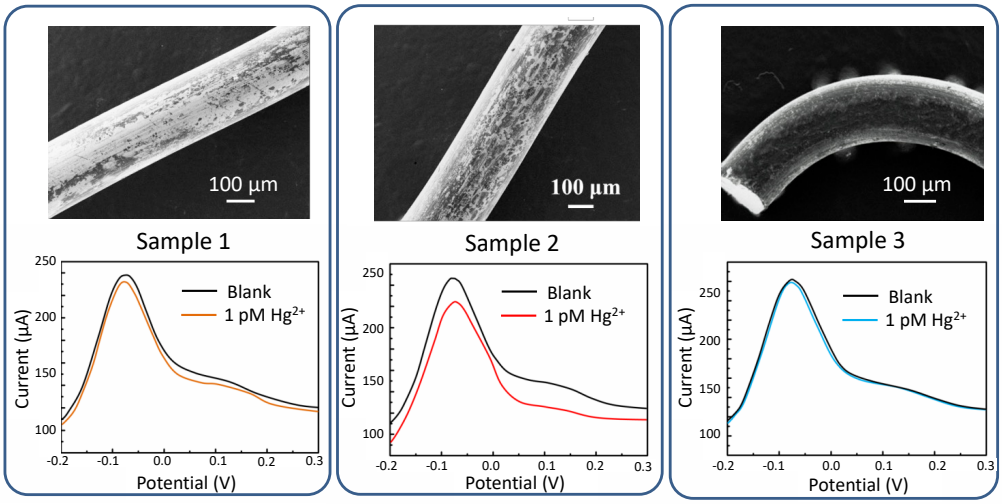

Figure 6. Top: SEM images demonstrating the rGO coverage differences of the three Cu/CuO/rGO/PPy samples. Bottom: the DPV curves of the fabricated Cu/CuO/rGO/PPy wires with different amount of rGO in the detection of 1 pM Hg^{2+} in phosphate buffer solution (PBS). Black curve – before adding Hg^{2+}; colored curves – after adding Hg^{2+}.

The prepared Cu/CuO/rGO/PPy wire (sample 2) was employed for the actual detection of Hg^{2+}. From the differential pulse voltammetry (DPV) curves (Figure 7a), it is observed that significant responses are achieved even if Hg^{2+} concentration is as low as fM level. As shown in the calibration curve (Figure 7b), the current response decreases with the increase of Hg^{2+} concentration, which is consistent with the above theoretical discussion. A wide linear range is obtained from 1 fM to 10 µM with the corresponding equation of the change of electrochemical current: $\Delta I = 2.516 \lg c + 51.5$, where c is the concentration of Hg^{2+} (in M). The lowest detection limit (LOD) is 0.25 fM (3σ method), which is significantly improved than other reported sensors (Table1). Moreover, the response is almost unchanged after 10 cycles in phosphate buffer solution (PBS), indicating good stability of the system (Figure S6).

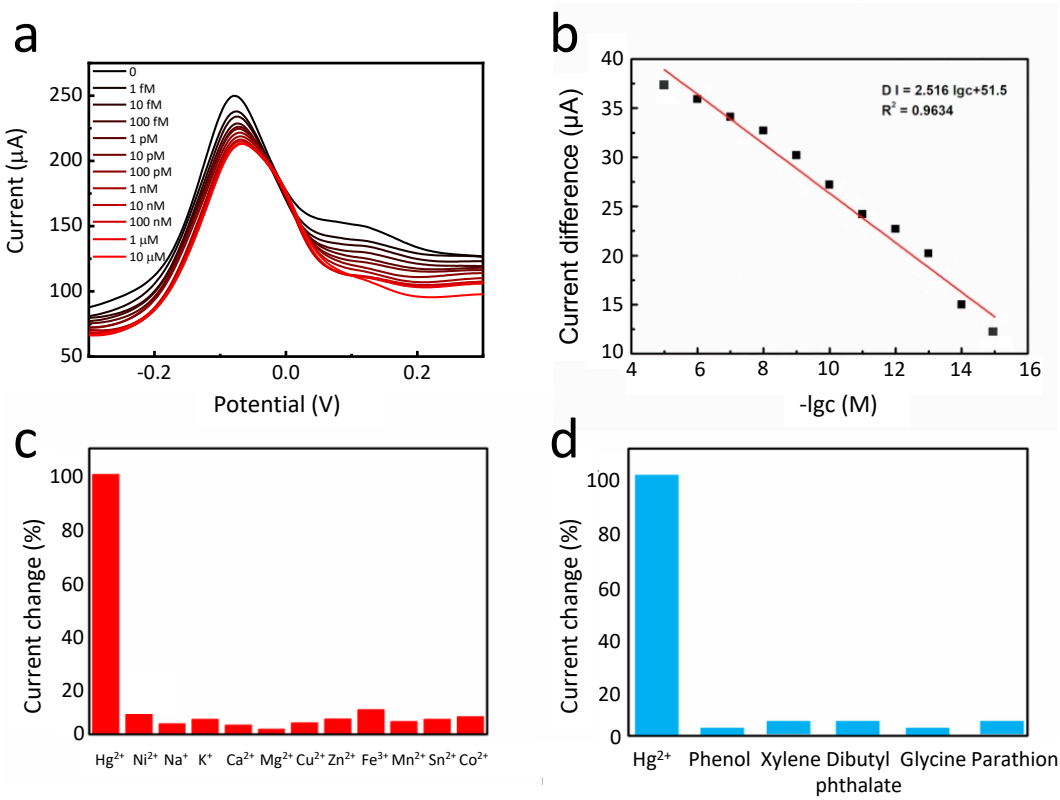

Figure 7. a) The DPV curves of the fabricated Cu/CuO/rGO/PPy wire in detection of Hg^{2+} in PBS. b) The calibration curve of Hg^{2+} concentrations versus peak current change. c-d) The anti-interference performance of the fabricated Cu/CuO/rGO/PPy wire in presence of common metal ions (c) and organic pollutants (d) with 100 times concentration (10 nM) of Hg^{2+}.

The anti-interference of the Cu/CuO/rGO/PPy wire was studied and the excellent performance was found. From Figure 7c-d, we can see that neither metal ions nor organic pollutants (with 100 times the concentration of Hg^{2+}) can cause any substantial interference to Hg^{2+} detection. The anti-interference is further tested in the actual seawater collected from the Yellow Ocean, China. As expected, the Cu/CuO/rGO/PPy wire exhibits a stable and efficient response to Hg^{2+} in seawater, and the recoveries of the added different concentrations of Hg^{2+} in real-life samples are statistically close to 100% with a deviation of less than 5% (Table S2). These results demonstrate the excellent anti-interference properties of the proposed sensing mode and the prototype sensor in seawater with high salinity and complex chemical components, which makes

the direct detection in seawater feasible. In addition, the robust structural features of the metal wire make it tolerate the hush environment of seawater in the practical application.

This excellent anti-interference performance of the new Φ_B-based sensing mode is mainly due to the following factors. First, the coated selective adsorption layer such as PPy or CS can eliminate the majority of the interference from the charged/uncharged species which cannot be specifically adsorbed onto the surface of the sensor. In these cases, $\Delta\Phi_B$ and the corresponding electrochemical response cannot be produced due to the lack of electrostatic induction. Second, since the energy barrier Φ_B cannot be disturbed by electrochemical redox, most electrochemical interferences are eliminated. Third, as discussed previously, the energy barrier can exponentially regulate the electrochemical response, while the redox interfering species can only influence the electrochemical response linearly. Therefore, the former will dominate the overall sensing signal.

To verify the universality of the energy-barrier-based sensing mode for anti-interference, further experiments with different recognizing layer for different analytes were carried out. The electrochemical detection of Cu^{2+} was further carried out by employing CS instead of PPy, as CS can selectively absorb Cu^{2+}.[29] It is found that the Cu/CuO/rGO/CS wire exhibits the significant electrochemical response to Cu^{2+}, while no obvious response can be observed from other metal ions or organic pollutants (Figure 8). Therefore, by changing the recognizing layer outside the energy-barrier layer, the novel sensing mode can be applied to detect other analytes.

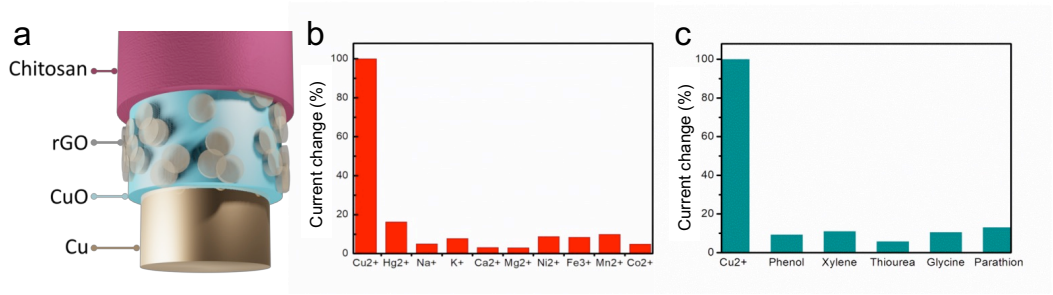

Figure 8. a) The schematic diagram of the Cu/CuO/rGO/CS wire. b-c) The anti-interference sensing performance of the fabricated Cu/CuO/rGO/CS wire in presence of common metal ions (b) and electrochemical active organic pollutants (c) with the same concentration (10nM).

In addition to the above used Schottky junctions, the energy barrier can also be formed by p-n junctions. As an example, NiO (a typical p-type semiconductor) and ZnO (a typical n-type semiconductor) can form a p-n junction barrier (Φ_{pn}) at the ZnO/NiO interface (Figure 9a). The fabricated Ni/NiO/ZnO wire with p-n junction interfaces affords a layer of Φ_{pn} (Figure 9b). For the negatively charged species absorbed on the exposed ZnO/NiO, this physical electrostatic interaction can lower the Φ_{pn} (as described in S1). This change of Φ_{pn} and its influence upon the electrochemical response were tested in the electrochemical sensing of DA. In this test, the addition of negatively charged Hb decreases Φ_{pn} through electrostatic interaction, which boosts the electrochemical response significantly (Figure 9c). Furthermore, Ni/NiO/ZnO/PPy wires were fabricated to build the Φ_{pn} based physical-electrochemical sensing mode and successfully used for the anti-interference detection of Hg^{2+} (Figure 9d). Therefore, similar to the Φ_B of Schottky junctions, the Φ_{pn} of p-n junctions can also be used as a tuning factor for electrochemical sensing, indicating the generality of the novel sensing mode.

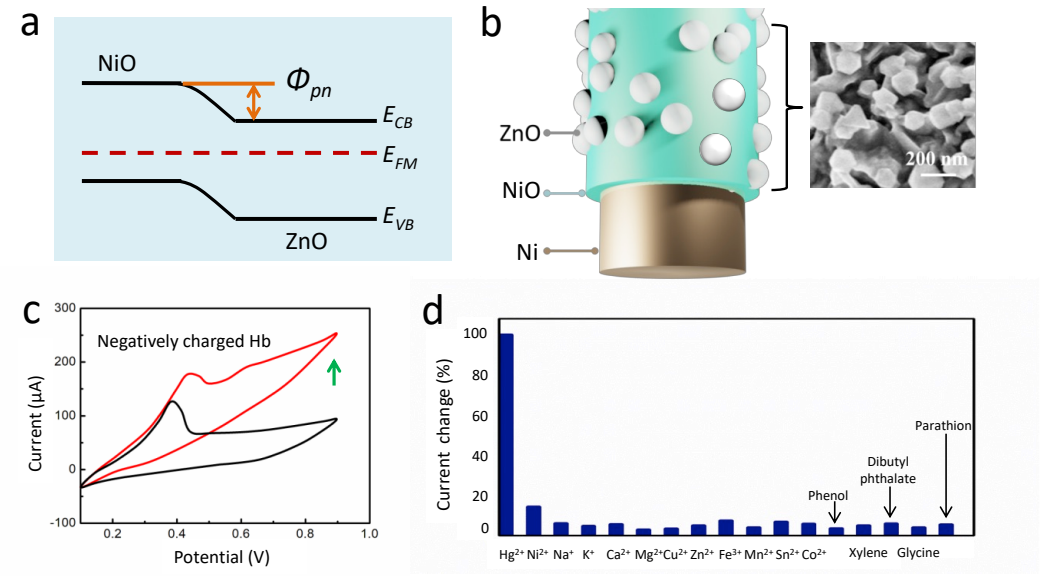

Figure 9. a) The schematic diagram of the Ni/NiO/ZnO wire and the SEM image of the surface. b) The energy band structures of NiO-ZnO p-n junction. c) The electrochemical response of the Ni/NiO/ZnO wire to the addition of negatively charged Hb. d) The anti-interference performance of the fabricated Ni/NiO/ZnO/PPy wire in presence of common metal ions and organic pollutants with 100 times concentrations (10 nM) of Hg^{2+}.

CONCLUSIONS

In conclusion, by constructing different hierarchical structures such as Cu/CuO/rGO/PPy, Cu/CuO/rGO/CS, and Ni/NiO/ZnO/PPy, we successfully introduced different interfacial energy barriers of Schottky or p-n junctions into the electrochemical sensors. Through the electrostatic interactions between the charged analytes and the interfacial junctions, the height of the energy barriers can be modified corresponding to the different charged analytes, which at last can be exponentially reflected in the electrochemical responses of the sensors. Different from the classic redox based electrochemical sensors, one of the most distinguishing properties of the new sensing mode based on the interfacial energy barrier is its anti-interference in complex scenarios such as in seawater. The specifically designed absorbing layer such as PPy for Hg^{2+} and CS for Cu^{2+} can accumulate analytes and their charges whose

electrostatic induction can influence the interfacial energy barrier even without involving redox. The good anti-interference properties and ultrahigh sensitivity of the new sensing mode offer new opportunities in trace analyte detection in harsh environments such as seawater.

METHODS

Synthesize of Cu/CuO wires: 1.14 g ammonium persulfate was added into 50 mL deionized water with stirring. After the above solution was dissolved completely, 5 g sodium hydroxide was added. After fully dissolving, the solution was cooled to room temperature. Cu wire (diameter 0.4 mm) was cleaned with acetone, ethanol and water by ultrasonic and then added into the above solution and kept for 15 min. After the reaction, the wire was taken out and cleaned by deionized water. It was then transferred into the electric drying oven at 180 ℃ for 3 h. Finally, the resultant Cu/CuO wire was taken out to the electric drying oven under 60 ℃ after natural cooling.

Synthesize of Cu/CuO/rGO wires: The graphene oxide (GO) prepared by modified hummer method [1] was firstly dissolved in deionized water and further sonicated to obtain the well-dispersed GO solution. The prepared Cu/CuO wire was cut into small sections and bent into a U shape. The electrodeposition of the reduced graphene oxide (rGO) was carried out in 1 mg/mL GO solution at −1.2 V by the three-electrode system, where a platinum plate as the counter electrode, an Ag/AgCl electrode as reference electrode and the Cu/CuO wire as the working electrode. After electrodeposition, the Cu/CuO/rGO wire was washed and dried.

Synthesize of Cu/CuO/rGO/PPy: For electrochemical polymerization of pyrrole,

2.6136 g sodium dodecylbenzene sulfonate (SDBS) was added into 50 mL deionized water to obtain the electrolyte solution. Electropolymerization was carried out in 0.1 M pyrrole monomer by cyclic voltammetric (from -0.5 V to 2 V) on a three-electrode system, and the Cu/CuO/rGO wire served as the working electrode. The loading amount of polypyrrole (PPy) was controlled by the number of potential scan cycles. After deposition, the Cu/CuO/rGO/PPy wire was washed and then dried.

Synthesize of Cu/CuO/rGO/CS wire: 0.5g Chitosan (CS) was added into 99.5 mL acetic acid aqueous solution and stirred for 1 h. Then, the Cu/CuO/rGO wire was soaked in CS solution and freeze-dried at -40 ℃ for 24 h after taking it out.

Synthesize of Ni/NiO/ZnO/PPy wire: 0.035 M $Zn(NO_3)_2 \bullet 6H_2O$, 38 mL deionized water and 2 mL $NH_3 \bullet H_2O$ were mixed to form a mixed solution. The cleaned Ni wire was added into the mixed solution in an autoclave and kept at 95 ℃ for 6 h, and then the composite Ni/NiO/ZnO wire was rinsed and dried at 60 ℃. The electrochemical polymerization of pyrrole is based on the above discussion.

Characterization and test: The morphologies of samples were characterized by scanning electron microscope (SEM). The X-ray diffraction (XRD) patterns of samples were characterized by a Bruker D8 ADVANCE X-ray diffractometer with Cu Kα radiation. The electrochemical experiments were carried out using a CHI600E workstation (Shanghai Chenhua) on a three electrode system in 0.1 M phosphate buffer solution (PBS) or seawater at room temperature. The seawater was collected from the Yellow Ocean at the coastal waters of Qingdao, China, and was filtered to remove the suspended solids without any chemical treatment.

■ ASSOCIATED CONTENT

* Supporting Information

The Supporting Information is available free of charge at

■ ACKNOWLEDGMENTS

This work was sponsored by National Natural Science Foundation of China (51602298) and Fundamental Research Funds for the Central University (841964011).

■ REFERENCES

(1) Rao, T.P.; Mentilda, P.; Gladis, J.M. *Crit. Rev. Anal. Chem.* **2005,** *35*, 247-288.

(2) Lee, P.L.; Sun, Y.C.; Ling, Y.C. *J. Anal. Atom. Spectrom.* **2009**, *24*, 320-327.

(3) Wang, N.; Lin, M.; Dai, H.; Ma, H. *Biosens. Bioelectron*. **2016**, *79*, 320-326.

(4) Lu, L.; Zhou, L.; Chen, J.; Yan, F.; Liu, J.; Dong, X.; Xi, F.; Chen, P. *ACS Nano*. **2018**, *12*, 12673-12681.

(5) Novillo, O.; Pertusa, J.F.; Tomás, J. *Sci. Total Environ*. **2017**, *598*, 1130-1139.

(6) Ding, L.; Zhao, M.; Fan, S.; Ma, Y.; Liang, J.; Wang, X.; Song, Y.; Chen, S. *Sensor Actuat. B-Chem.* **2016**, *235*, 162-169.

(7) Pizarro, J.; Flores, E.; Jimenez, V.; Maldonado, T.; Saitz, C.; Vega, A.; Godoy, F.; Segura, R. *Sensor Actuat. B-Chem.* **2018**, *281*, 115-122.

(8) Cui, L.; Wu, J.; Ju, H. *Biosens. Bioelectron.* **2015**, *63*, 276-286.

(9) Yue, H.; Huang, S.; Chang, J.; Heo, C.; Yao, F.; Adhikari, S.; Gunes, F.; Liu, L.; Lee, T.H.; Oh, E.S.; Li, B.; Zhang, J.; Huy, T.Q.; Luan, N.V.; Lee, Y.H. *ACS Nano*. **2014**, *8*, 1639-1646.

(10) Gong, J.; Antonietti, M.; Yuan, J. *Angew. Chem. Int. Ed*. **2019**, *56*, 7557-7563.

(11) Yan, H.; Xie, Y.; Jiao, Y.; Wu, A.; Tian, C.; Zhang, X.; Wang, L.; Fu, H. *Adv. Mater*. **2018**, *30*, 1704156.

(12) Hao, Z.; Shen, Z.; Li, Y.; Wang, H.; Zheng, L.; Wang, R.; Liu, G.; Zhan, S. *Angew. Chem. Int. Ed.* **2019**, *58*, 6351-6366.

(13) Tian, B.; Cohen-Karni, T.; Qing, Q.; Duan, X.; Xie, P.; Lieber, C.M. *Science*. **2010**, *329*, 830-834.

(14) Lu, B.; Zeng, S.; Li, C.; Wang, Y.; Pan, X.; Zhang, L.; Mao, H.; Lu, Y.; Ye, Z. *Carbon*. **2018**, *132*, 191-198.

(15) Zhang, K.; Liu, C.; Huang, F.; Zheng, C.; Wang, W. *Appl. Catal. B*. **2006**, *68*, 125-129.

(16) Yu, R.; Niu, S.; Pan, C.; Wang, Z. *Nano Energy*. **2015**, *14*, 312–339.

(17) Guo, L.; Yang, Z.; Dou, X. *Adv. Mater*. **2017**, *29*, 1604528.

(18) Cao, X.; Cao, X.; Guo, H.; Li, T.; Jie, Y.; Wang, N.; Wang, Z. *ACS Nano*. **2016**, *10*, 8038–8044.

(19) Hu, Y.; Zhou, J.; Yeh, P.H.; Li, Z.; Wei, T.Y.; Wang, Z. *Adv. Mater.* **2010**, *22*, 3327–3332.

(20) Wang, Z.; Xiao, Y.; Cui, X.; Cheng, P.; Wang, B.; Gao, Y.; Li, X.; Yang, T.; Zhang, T.; Lu, G. *ACS Appl. Mater. Interfaces.* **2014**, *6*, 3888−3895.

(21) Guo, F., The Researches on Current Saturation Properties of ZnO Nanowire Schottky Barrier, Master's Thesis, 2014.

(22) Nam, C.; Tham, D.; Fischer, J, Nano Lett., **2005**, 5 (10), 2029-2033.

(23) Das, S.N.; Choi, J.-H.; Kar, J.P. et al., Appl. Phys. Lett., **2010**, 96 (9), 092111.

(24) Chen, C.; Zhang, J.; Adivarahan, V. et al., Appl. Phys. Lett., **2003**, 82 (25), 4593-4595.

(25) Yeh, P.H.; Li, Z.; Wang, Z. *Adv. Mater*. **2009**, *21*, 4975-4978.

(26) Zhao, M.; Cai, B.; Ma, Y.; Cai, H.; Huang, J.; Pan, X.; He, H.; Ye, Z. *Nanoscale*. **2014**, *6*, 4052-4057.

(27) Chandra, V.; Kim, K.S. *Chem. Commun*. **2011**, *47*, 3942-3944.

(28) Ballav, N.; Das, R.; Giri, S.; Muliwa, A.M.; Pillay, K.; Maity, A. *Chem. Eng. J*. **2018**, *345*, 621–630.

(29) Wang, B.; Bai, Z.; Jiang, H.; Prinsen, P.; Luque, R.; Zhao, S.; Xuan, J. *J. Hazard. Mater.* **2019**, *364*, 192-205.

(30) Safavi, A.; Farjami, E. *Anal. Chim. Acta*. **2011**, *688*, 43-48.

(31) Abollino, O.; Giacomino, A.; Malandrino, M.; Piscionieri, G.; Mentasti, E. *Electroanal*. **2008**, *20*, 75-83.

(32) Wang, F.; Wei, X.; Wang, C.; Zhang, S.; Ye, B. *Talanta*. **2010**, *80*, 1198-1204.

(33) Filho, N.L.D.; Carmo, D.R.; Rosa, A.H. *Electrochim. Acta*. **2006**, *52*, 965-972.

(34) Lin, Y.; Peng, Y.; Di, J. *Sensor Actuat. B-Chem.* **2015**, *220*, 1086-1090.

(35) Lu, X.; Dong, X.; Zhang, K.; Zhang, Y. *Anal. Methods*. **2012**, *4*, 3326-3331.

(36) Zhou, N.; Chen, H.; Li, J.; Chen, L. *Microchim. Acta*. **2013**, 180, 493-499.

(37) Fu, X.; Wu, J.; Ni, L.; Cheng, G.; Liu, J.; Huang, X. Anal. *Chim. Acta*. **2012**, *720*, 29-37.

(38) Wu, Z.; Jiang, L.; Zhu, Y.; Xu, C.; Ye, Y.; Wang, X. *J. Solid State Electrochem*. **2012**, *16*, 3171-3177.

(39) Gong, J.; Zhou, T.; Song, D.; Zhang, L.; Hu, X. *Anal. Chem.* **2009**, *82*, 567-573.

Table 1. Comparison of the sensing performance of various electrode materials to Hg^{2+}.

Electrode materials	LOD	Electrolyte solution	Ref.
Cys-Au NPs-CILE	2.3nM	0.1M PBS	30
Au NPs–GCE	7.5pM	0.06M HCl	31
p-tert-butylthiacalixarene	200pM	0.01M KCl	32
SIAMT–CPE	500pM	0.05M KNO_3	33
np-Au NPs/ITO	150pM	0.1M HCl	34
ssDNA/Au NPs/CNT/GC	30pM	0.01M PBS	35
MTU/Au NPs/GO/ITO	780pM	0.1M KCl	36
PMBT/Au NPs/CNTs/GC	80pM	0.01M HNO_3/KCl	37
NiO-CH/GCE	40pM	0.1M PBS	38
Au-PtNPs/NF	40pM	1M HCl	39
Cu/CuO/rGO/PPy	0.25fM	0.1M PBS	This work